Waveform based Inverse Kinematics Algorithm of Kinematically Redundant 3-DOF Manipulator

Setyamartana Parman [*a1], **Affiani Machmudah** [b2]

[1]Fakulti Teknologi Kejuruteraan Mekanikal dan Pembuatan
Universiti Teknikal Malaysia Melaka, 75450 Ayer Keroh, Melaka, Malaysia

[2]Fakultas Sains dan Teknologi,
Universitas Airlangga, Jalan Mulyosari, Surabaya 60115, Indonesia

[*a] setyamartana@utem.edu.my; [b] affiani.machmudah@fst.unair.ac.id

ABSTRACT

This paper presents a new approach to the problem of inverse kinematics by modelling robot arm movements as signals generated from algebra-based solutions. The inverse kinematics of point $P(x_P, y_P)$ are modelled as sinusoidal functions with mechanical constraints. Unique wave forms occur at each point in the workspace. There are four types of inverse kinematic waves depending on how sinusoidal waves cross the value of mechanical constraints. In terms of tracking the path, the robot's arm produces complex waves that produce the desired movement. Due to mechanical constraints, many points in the workspace have the bandwidth where the signal is produced only at limited intervals from the angular domain. Tracks must be stored at these appropriate intervals, which build bandwidth tunnels, completely from the initial configuration to the final configuration. Simulations will be carried out using 3-DOF series planar robots to track highly complex mathematical curves. With a wave-based approach, the solution of the IK problem can benefit from wave characteristics such as the superposition principle.

Keywords: Waveform; sinusoidal function; inverse kinematics algorithm; kinematically redundant manipulator.

1. INTRODUCTION

Robot arm manipulators have been used in industrial applications to pick and place assignments. Moreover, they have also been implemented to carry out advanced jobs those are operated in very complex environments. To carry out their assignments, their paths must be planned well using an offline or online algorithm. The offline path tracking algorithm then gained the highest popularity compared to the online algorithm because the online algorithm is only suitable for simple work [1-2].

In terms of tracking curves with a robot arm, it is necessary to complete the Inverse Kinematics (IK) for all curves that are tracked. Research in completing the IK arm robot is a long-term journey that has been carried out since in the last four decades [3]. Almarkhi et al [4] investigated kinematic redundant manipulators to reduce a single configuration. Programming and control techniques to overcome redundancy are also discussed. The IK function approach by constructing mathematical functions to model joint path angles has been presented by Wampler [5]. In 1985, Baillieul proposed Jacobian to solve the IK problem [6]. Barker et al. [7] discusses several tracking algorithms, including the inverse function approach, minimum norm methods, methods

that involve optimization of potential functions and extended Jacobian methods. Three theorems have been given regarding the problem of defining the IK algorithm and the cycle behavior of the tracking algorithm. Burdick [8] uses the concept of independent motion types as a global solution for IK.

At present, many approaches have been proposed to solve IK problems analytically and numerically [3, 9-18]. Ahuactzin et al [9] proposed a method, namely a kinematic road map, to resolve IKs from overly excessive manipulators. Nearchou et al [10] propose a modified Genetic Algorithm (mGA) for IK of a redundant manipulator in a barrier environment. Marcos et al [11] proposed to resolve IK from a redundant manipulator by controlling the joint position using a closed loop pseudo-inverse combining with a multi-objective genetic algorithm. Interval analysis has been used also in solving IK problems [12-17]. Wei et al [14] developed the weighted space vector projection method as a general approach to solving IK nR robots. An approach using a fully automatic planar curve has been proposed to solve the IK problem of a common 6-DOF serial manipulator [15].

Welding robot is one robot that must follow the path perfectly. For shipbuilding, welding of the double hull structure is currently carried out by experienced workers. The duration for completing work by human operators takes a very long time; around eight months [19]. Manipulators can be used as part of robotic systems in tracking welding paths for shipbuilding and other difficult geometries. The task is naturally conveyed in Cartesian coordinates while the movements carried out in shared coordinates are one of the main problems responsible for the complexity of robot arm movements. For welding purposes, a very accurate position is needed so that in tracking the manipulator paths from very complex geometries, a new approach in the IK algorithm that can overcome this position error needs to be developed.

Sinusoidal functions are extraordinary mathematical equations that have succeeded in explaining extremely difficult phenomena. In the electromagnetic field, he described the characteristics of light waves. Sinusoidal waves also have a very important role in science and engineering. They are the building blocks of the Fourier series that have succeeded in analysing difficult phenomena in various subjects.

This paper will show that sinusoidal waves are also present in robot arm movements. Because robots are mechanical devices, the waves generated are limited by mechanical constraints. Depending on the position of the point being tracked in the workspace, the resulting signal can be either fully sinusoidal or truncated sinusoidal. IK's research interests focus on avoiding singularities and minimizing positional errors. By using the IK wave model, the signal will be generated either as a continuous signal or a signal with angular domain bandwidth. This bandwidth will build the right regional tunnel when tracking the path. Tracks must be stored in this bandwidth tunnel. Because the IK wave model was developed from an algebra based solution, zero error in position can be achieved.

2. SINUSOIDAL FUNCTION WITH MECHANICAL CONSTRAINT

The 3-DOF Planar series robots have analytic solutions using algebraic methods. There is an algebraic variable, namely the global angle θ_g. To get basic knowledge about IK waveform of robot movements, the analysis in this paper is carried out when the robot arms have no joint limits. The IK 3-DOF planar robot problem has the following algebraic solution

$$w_x = x_p - l_1 \cos(\theta_g) \tag{1}$$

$$w_y = y_p - l_1 \sin(\theta_g) \tag{2}$$

$$c_{2P} = \frac{\left(w_x{}^2 + w_y{}^2 - l_1{}^2 - l_2{}^2\right)}{2l_1 l_2} \tag{3}$$

$$s_{2P} = \pm\sqrt{1 - c_{2P}{}^2} \tag{4}$$

$$\theta_2 = a\tan 2(s_{2P}, c_{2P}) \tag{5}$$

where (x_p, y_p), l_1, l_2, l_3, θ_2, c_{2P}, s_{2P}, are the position of end-effector in Cartesian coordinate, the first link length, the second link length, the third link length, the second joint angle, the cosines of θ_2, the and sine of θ_2, respectively.

Second and third joint angles can be obtained by following equations

$$\Delta = w_x{}^2 + w_y{}^2 \tag{6}$$

$$s_{1P} = \frac{(l_1 + l_2 c_{2P})w_y - (l_2 s_{2P} w_x)}{\Delta} \tag{7}$$

$$c_{1P} = \frac{(l_1 + l_2 c_{2P})w_x + (l_2 s_{2P} w_y)}{\Delta} \tag{8}$$

$$\theta_1 = a\tan 2(s_{1P}, c_{1P}) \tag{9}$$

$$\theta_3 = \theta_g - \theta_2 - \theta_1 \tag{10}$$

where θ_1, c_{1P}, s_{1P}, and θ_3 are the first joint angles, the cosine of θ_1, the sine of θ_1, and the third joint angle, respectively. The sine wave is an elementary waveform in nature. It occurs in many cases of physics, mathematics, and engineering. It also appears in the arm robot motion as the analytic solution of inverse position.

Substituting (1) and (2) to (3) and using trigonometric function analysis, the following equation can be obtained :

$$c_{2P} = A_x \cos\theta_g + A_y \sin\theta_g + k_p = A_p \cos(\theta_g - \varphi_p) + k_p \tag{11}$$

$$-1 \le c_{2P} \le 1 \tag{12}$$

$$A_x = \frac{-l_3 x_p}{l_1 l_2} \qquad A_y = \frac{-l_3 y_p}{l_1 l_2} \tag{13}$$

$$A_p = \sqrt{A_x{}^2 + A_y{}^2} = \frac{l_3}{l_1 l_2} R \tag{14}$$

$$\phi_P = a\tan 2(A_y, A_x) \tag{15}$$

$$k_p = \frac{R^2 + l_3{}^2 - l_2{}^2 - l_1{}^2}{2l_1 l_2} \tag{16}$$

$$R = \sqrt{x_p{}^2 + y_p{}^2} \tag{17}$$

where ϕ_p, K_p, A_p, and R are a phase angle, a center line of amplitude, an amplitude, a radius from the fix base, respectively. Eq. (11) is the general equation of the sinusoidal function. Due to Eq. (4), the values of this sinusoidal wave are limited from -1 to 1 as described in Eq. (12). c_{2P} as solution of IK is the sinusoidal function, as expressed in (11), with the mechanical constraint, as shown in (12). c_{2P} value depends on the radius, R, the global angle, and the links length: l_1, l_2, and l_3. The waveform of arm robot motion lies in the interval [-1, 1] because of the mechanical constraint. This mechanical constraint will be presented in Section 3.3.

Figure 1 shows c_{2P} graph when the mechanical constraint is not considered. Without mechanical constraint, the graph will be a fully sinusoidal function. Figure 2 shows the detail of the sinusoidal graph of c_{2P} for different radius and position angle. For point

$P(x_P,y_P)$, with radius R and angle ψ from x-axis, as shown in Figure 3(a), $\theta_P \pm k \cdot 2\pi$ are feasible since it satisfies the condition in Eq.(11). Figure 3(b) is sinusoidal graph for specific point $P(x_P,y_P)$. Figure 3(c), shows the postures formed by $\theta_P \pm k \cdot 2\pi$.
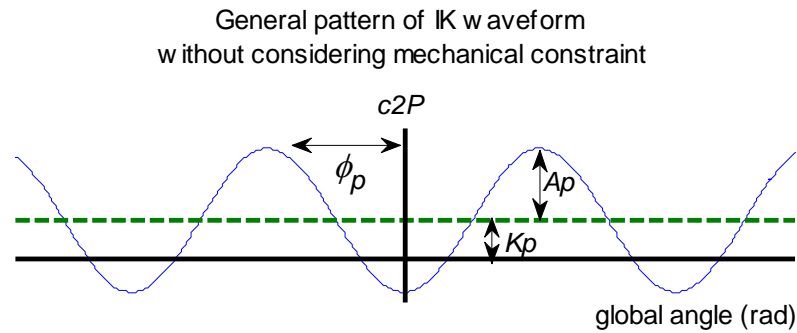
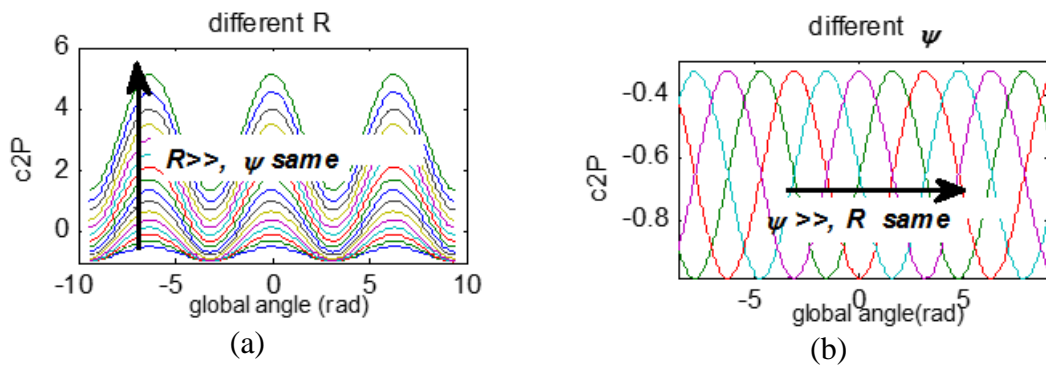General pattern of IK waveform
without considering mechanical constraint

Figure 1. Sinusoidal function of IK waveform without considering mechanical constraint

Figure 2. Variation of c_{2P}: (a) at constant ψ, (b) at constant R.
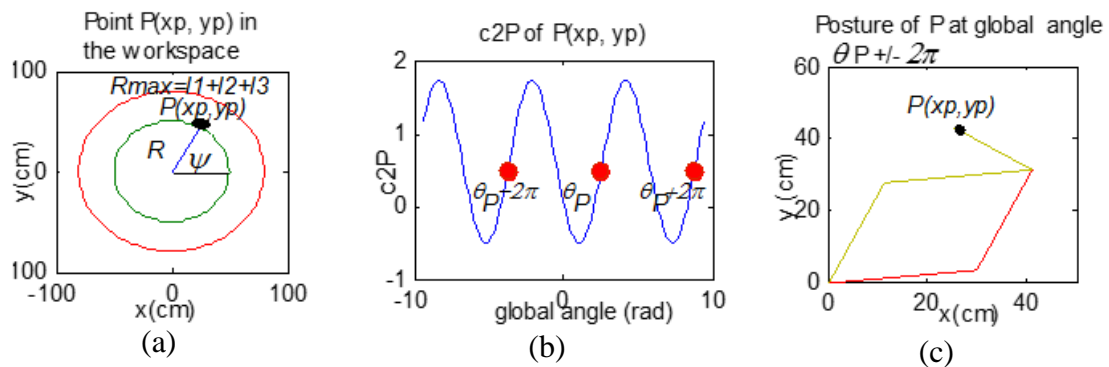
Figure 3. (a) Representation of $P(x_p, y_p)$ (b) Variation of c_{2P} of $P(x_p, y_p)$ (c) Physical meaning of choosing θ_g

The robot arms have the capability to generate sinusoidal functions at point $P(x_P,y_P)$. However, it has mechanical limitations as shown in Eq. (12) so that some points in the workspace will generate the waveforms at limited intervals or domain angle bandwidths. The details of IK waveforms will be discussed in the next section.

3. INVERSE KINEMATICS WAVEFORM

Signals are defined as functions that perform information about system characteristics [20]. For robot arms, the signal conveys information about how to make the desired movement. Understanding the signal nature of the motion of a robot arm is very important to avoid positioning errors. Before heading to position error analysis, the phenomenon of singular configuration, which is very important in the movement of a robot arm, will be investigated first.

3.1 Singularity Configurations

Figures 4(a) and 4(c) show an example of two single configurations for a 3-DOF planar robot as one robot that is kinematically redundant. Figures 4(b) and 4(d) are the IK waveforms of this single configuration. This shows that Figure 4(c) is possible to avoid because there are other tracks in the appropriate area. In this case, the singular configuration can be prevented by avoiding global angles that have a c_{2P} value equal to -1 or 1.
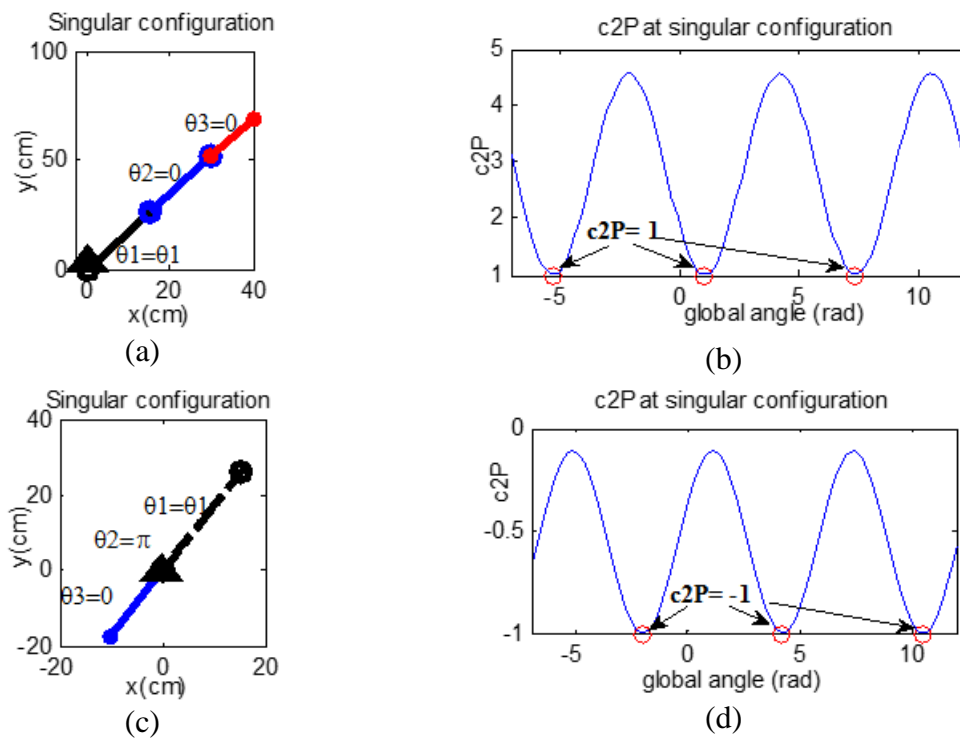
Figure 4. Single and c2P configurations.

3.2 Bandwidth of the Angular Domain

There are many global angles that give c_{2P} equal to -1 and 1. To track point $P(x_P, y_P)$, choosing an angle that gives c_{2P} beyond the interval [-1, 1], means there will be a position error. Thus, keeping c_{2P} inside [-1, 1] is a condition needed to track a path with zero error position. The concept of bandwidth is present in many subject areas from computer networks, signal processing, spectroscopy to graph theory. This paper will show that the concept of bandwidth is very important in IK to achieve zero error in position during curve tracking.

Using Eq.(10), the 3-DOF planar robot self-motion can be modelled as a function of the following interval values.

For $P(x_P, y_P)$:

$$\theta_g = \theta_1 + \theta_2 + \theta_3$$
$$\theta_1 = [\theta_{1\min}, \theta_{1\max}]$$
$$\theta_2 = [\theta_{2\min}, \theta_{2\max}] \tag{18}$$
$$\theta_3 = [\theta_{3\min}, \theta_{3\max}]$$

With this approach, θ_g this is a function of variables θ_1, θ_2 and θ_3 where they are real numbers in radians with certain intervals.

For $P(x_P, y_P)$, reasonable angular domain intervals can be calculated by solving the following inequalities

$$|c_{2P}| \leq 1$$
$$-1 \leq c_{2P} \leq 1$$
$$-1 \leq A_p \cos(\theta_g - \varphi_p) + k_p \leq 1 \tag{19}$$
$$-\frac{1 - k_p}{A_p} \leq \cos(\theta_g - \varphi_p) \leq \frac{1 - k_p}{A_p}$$

Solve the equation for θ_g, domain angle intervals from the minimum angle to the maximum angle, $\theta_g = [\theta_{g\,\min}, \theta_{g\,\max}]$, as a limited interval can be obtained. Point $P(x_P, y_P)$ will produce a signal only at this angular domain interval. This special interval is the bandwidth of the angular domain where the signal is only available in this global band.
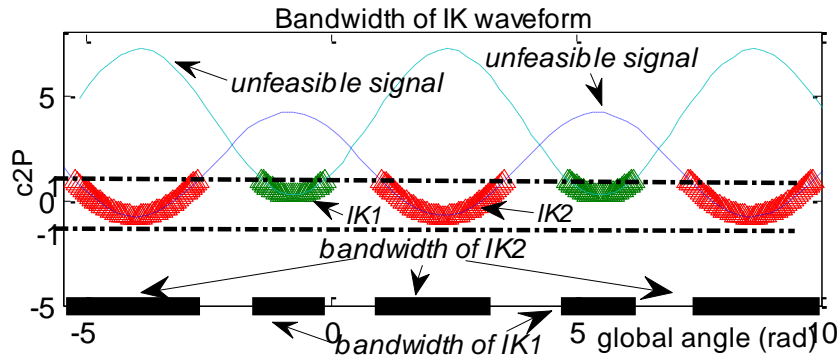
Figure 5. Bandwidth of the angular domain.

3.3 IK Waves from Point $P(x_P, y_P)$

The general pattern of a robot arm's signal depends on the characteristics of the robot: l1, l2, and l3. Different link lengths have different waveform patterns. It's important to know the possibility of IK wave patterns. There are four types of IK waves depending on how the sinusoidal graph intersects $c_{2P} = 1$ and $c_{2P} = -1$. This section will present these IK wave types in detail.

The first possible pattern of IK waveforms is type I as shown in Figure 6. Waveform is a fully sinusoidal function. For this waveform, all the generated signals are at [-1, 1] so there is no mechanical obstacle to reach this point in the workspace. Signals can be generated for all global angles: $\theta_g \in R$.

The second possible pattern is type II. This happens when the sinusoidal graph crosses $c_{2P} = 1$ only. Sinusoidal signal truncated with limited bandwidth from the angular domain. The waveform shown in Figure 5 is an illustration of this type. Physically, type II waveforms represent the postures that can be produced to reach point $P(x_P, y_P)$ as shown in Figure 7. Solving inequality Eq.(19), the minimum and maximum global angles create maximum / minimum postures that geometrically form concave / convex

kite as shown in Figure 8(a). Figure 8(b) shows details of the posture that may originate from a positive root sign in Eq.(4) while Figure 8(c) is a posture detail that allows for a negative root sign in Eq.(4).
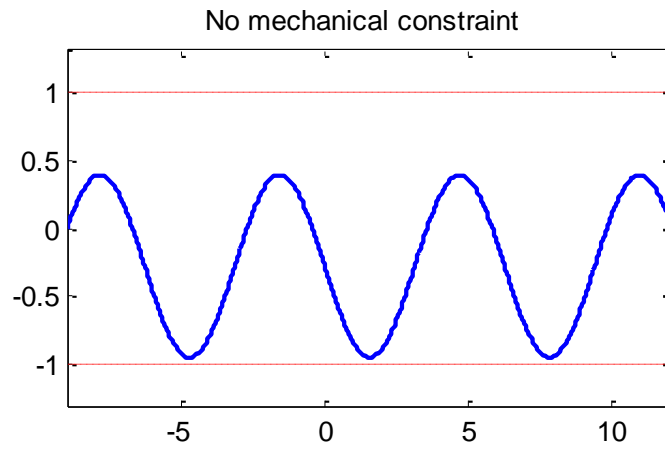

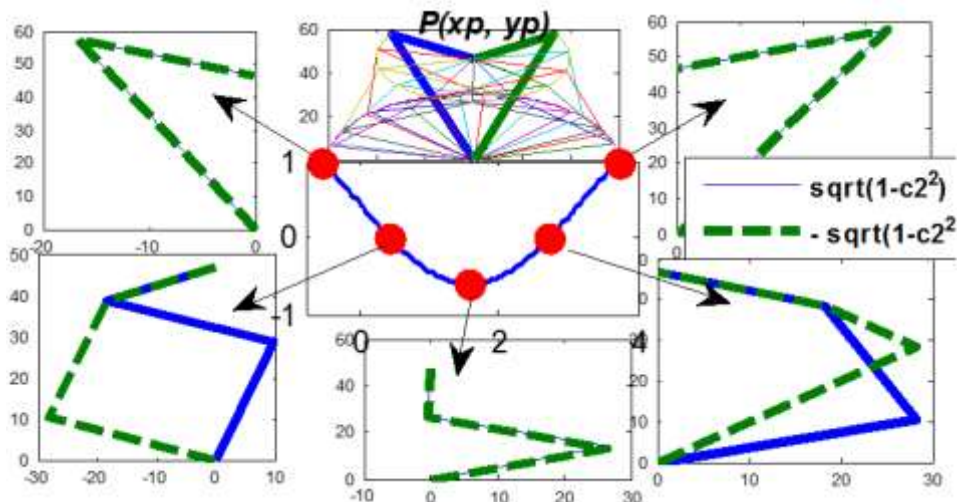Figure 6. Type I: IK waveforms are fully sinusoidal functions.

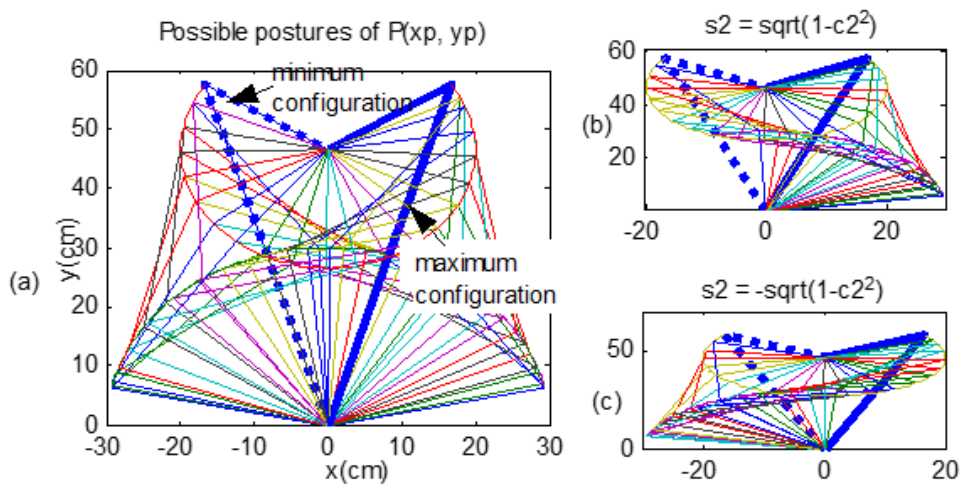Figure 7. IK waveforms represent all possible postures to reach the point $P(x_P, y_P)$.

Figure 8. (a) Posture for point $P(x_P, y_P)$, (b) $s_{2P} = \sqrt{1 - c_{2P}^2}$, and (c) $s_{2P} = -\sqrt{1 - c_{2P}^2}$.

The third possible c_{2P} graph is type III as illustrated in Figure 9. In this case, the bandwidth occurs because the c_{2P} graph crosses both, $c_{2P} = 1$ and $c_{2P} = -1$. Unlike the type II waveforms, for type III, the maximum / minimum posture does not make the kite perfect as shown in Figure 10.
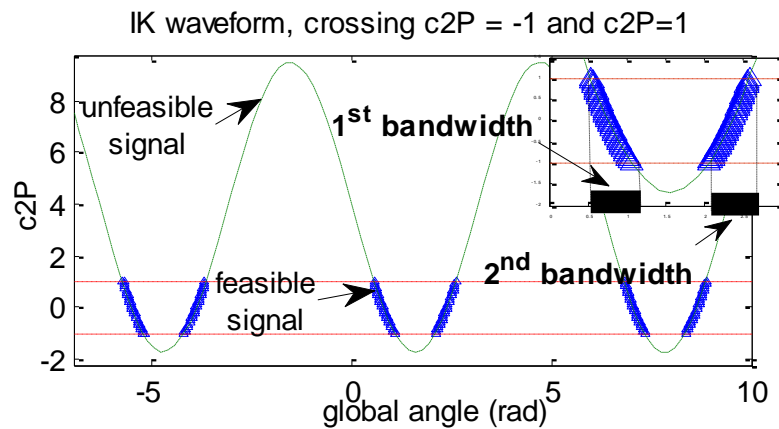

Figure 9. Type III: IK waves when sinusoidal functions cross $c_{2P} = -1$ and $c_{2P} = 1$.

Figure 10. Possible posture for the point $P(x_P, y_P)$ when the sinusoidal function crosses $c_{2P} = -1$ and $c_{2P} = 1$.

Another possible c_{2P} graph is type IV. The bandwidth of the angular domain is formed when a sinusoidal wave crosses $c_{2P} = -1$ only as shown in Figure 11. Figure 12 shows the mechanical representation of this waveform.
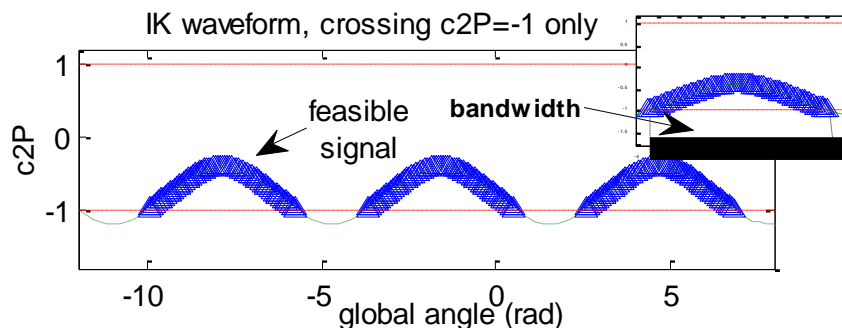

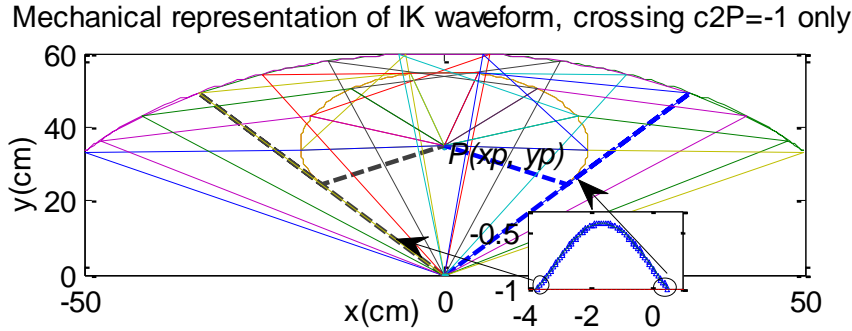Figure 11. Type IV: IK waves when sinusoidal function crosses $c_{2P} = -1$ only.

Figure 12. Possible posture for the point $P(x_P, y_P)$ when the sinusoidal function crossing c_{2P} =-1 only.

4. TRAJECTORIES GENERATION IN ANGLE DOMAIN

IK waveform types have been presented in previous section. Depending on the length of the link and the position of the point in the workspace, the IK wave signal will be formed. Signals will be generated at certain intervals, except for type I.

4.1 Angular Path Uses Continuous Functions

After the correct area of track tracking is obtained, the next problem is how to create tracks in this proper domain. The path can be generated from the initial angle to the final angle using a continuous function. This paper will use the sixth degree polynomial as a global angular trajectory because using this function as a trajectory only needs one unknown variable to determine. The boundary conditions used are the initial known global angle, the known final global angle, initial zero global speed, final zero global speed, and initial zero global speed, and final zero global speed.

The sixth level polynomial has the following general formula

$$\theta_g(r) = a_{6g}r^6 + a_{5g}r^5 + a_{4g}r^4 + a_{3g}r^3 + a_{2g}r^2 + a_{1g}r + a_{0g} \tag{20}$$

Where θ_g, r and a_{ng} are global angular trajectories, linear time scales, nth polynomial coefficients, respectively.

Substituting known and boundary conditions, the following equation can be obtained

$$a_{og} = \theta_i \ ; \ a_{1g} = a_{2g} = 0; \tag{21}$$

$$a_{5g} = -3a_{6g} - 6\theta_{gi} + 6\theta_{gf} \tag{22}$$

$$a_{4g} = 0.5(-9a_{6g} - 5a_{5g}) \tag{23}$$

$$a_{3g} = \theta_{gf} - \theta_{gi} - a_{6g} - a_{5g} - a_{4g} \tag{24}$$

where θ_{gi} and θ_{gf} are the initial and final global angles, respectively.

Substituting the above equations into Eq.(20), the global angular trajectory can be written in the following form

$$\theta_g(r) = a_{6g}r^6 + a_{5g}r^5 + a_{4g}r^4 + a_{3g}r^3 + a_{0g} \tag{25}$$

The unknown variable is the sixth polynomial coefficient, a_{6g}. Figure 14 shows global angular trajectory patterns for different a_{6g} values. The trajectory will be limited to r from 0 to 1 because of the linear time scale value.
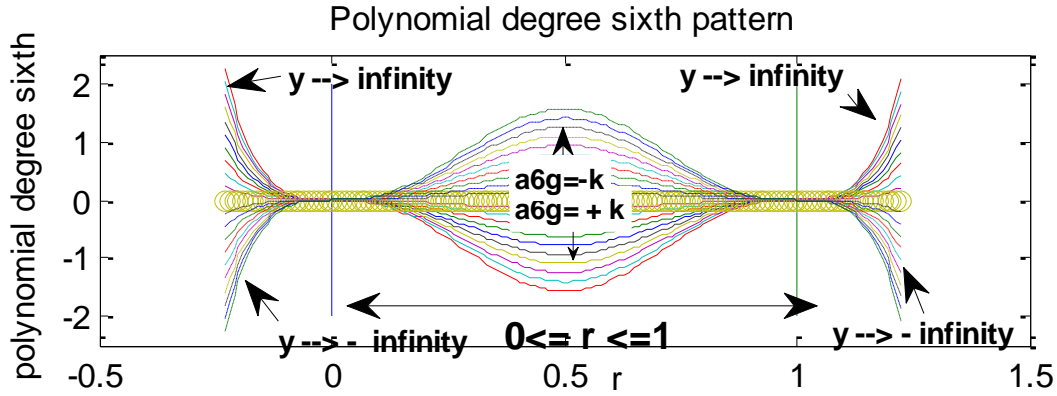
Figure 14. Pattern of the sixth degree polynomial coefficient.

4.2 Mapping the Paths into the Bandwidth Tunnel

To track a curve, the bandwidth of the angle domain must be calculated completely from the starting point to the end point. This procedure will build an angular bandwidth tunnel. Bandwidth tunnels are a feasible domain for track tracking. By keeping the global angle value in this tunnel will avoid mistakes in its position.

The feasible track region can be clearly seen by mapping the sixth polynomial level into the bandwidth tunnel. First, the initial and final global angles must be selected in the intervals before replacing them with Eqs.(21)-(25). Sixth degree polynomials that have parts outside the tunnel are prohibited because they will give an error in their position. Figure 15 shows an example of trajectory generation in the angular domain.
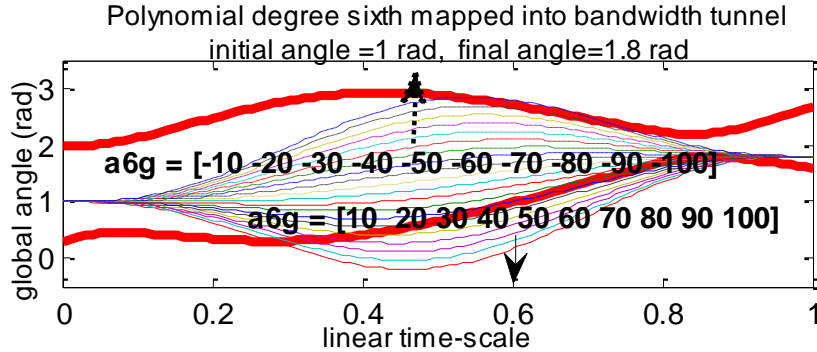

Figure 15. Example of trajectory generation in the angular domain: Sixth degree polynomial mapped into tunnel bandwidth for $\theta_{gi} = 1$ rad and $\theta_{gf} = 1.8$ rad.

4.3 Generated Waves of Path Tracking

To track a path, the Cartesian path, $P(x_P, y_P)$, continues to change from the starting point to the end point. For robot arms with a constant link length, amplitude, phase angle, and k will change according to the value $P(x_P, y_P)$. Thus, it will produce complex waves. The problem becomes how to choose global trajectories because they may lie at certain intervals only according to the IK waveforms of the Cartesian path.

The waveform of the curve traced as a function of time can be expressed as a composition function as follows

$$c_2(t) = \left(A\cos(\theta_g - \alpha) + k\right) o\, \theta_g\left(r\right) o\, r(t)$$

$$-1 \le c_2(t) \le 1$$

(26)

5. INVERSE KINEMATICS ALGORITHM

According to the analyses have been presented previously, the IK algorithm for manipulator path tracking can be computed using the following procedure

1. Solving inequality of mechanical constraint, Eq.(19), to compute the periodic bandwidth of the angle domain
2. Make interval-limited as band of interest. Since the waveform is periodic so that the bandwidth is also periodic, the interval-limited is used as an interval of interest. The analysis will be focused at this interval to avoid an ambiguity of values of the angle domain trajectories.
3. Map the trajectories of $\theta_{g\min}$ and $\theta_{g\max}$ completely from the initial configuration to the final configuration. It will construct the bandwidth tunnel.
4. Generating the trajectories inside this tunnel to avoid the position error and singularity configuration

6. NUMERICAL EXPERIMENTS FOR 3-DOF PLANAR ROBOT

A simulation in MATLAB has been conducted, by coding in m-file. The 3-DOF planar series robot will be used to track the complex paths using IK waveform model.

6.1 Effect of +/- Sign of Initial and Final Global Angles

This section will investigate very interesting motion planning result in [21]. In their paper, Machmudah et al has shown that different sign of initial and final joint angles has given a significant effect in the avoiding collision path, although physically, they represent same initial/final posture.

The Cartesian path and the value of a_{6g} resulted from [21] will be analyzed using IK waveform model. Detail of the end effector path is provided in Table 1, while Table 2 presents the data of the initial and the final configuration used in [21]. The path from PSO will be used since it has best result according to [21]. Appendix A illustrates the obstacle coordinates used in this path planning.

The waveform pattern of the arm robot with $l_1 = 30$cm, $l_2 = 30$cm, and $l_3 = 20$cm is shown in Figure 16. This arm robot generates two types of waveform, type I and type II only. Following the IK algorithm, the bandwidth tunnel of the avoiding collision path from PSO result is illustrated in Figure 17. This tunnel is calculated without considering the obstacle effect. The θ_g trajectories can be mapped into this tunnel. Figure 17 shows that the PSO trajectories are inside the tunnel.

Table 1. Cartesian path analyzed, source [21].

	a_{61}	a_{62}	a_{63}	$a_{6g}=a_{61}+a_{62}+a_{63}$
PS0	118.5065	-104.7164	18.8116	32.602

Table 2. Global angle, source [21].

	θ_1 (rad)	θ_2(rad)	θ_3(rad)	$\theta_g=\theta_{1}+\theta_{2}+\theta_3$
Initial	4.8200	0.1211	1.2944	6.2355
Final	0.35078	1.2689	6.0689	7.6886

Since c_{2P} is periodic function, the tunnel is also periodic as illustrated in Figure 18. Using a_{6g} from PSO trajectories, the postures change from starting point to final point is illustrated in Figure 19. There are two possibilities of posture change since the root of Eq. (4) can be positive or negative. Negative root gives the motion of the link which

collides with obstacle. Thus, for next analysis, the result form positive sign of root in Eq. (4) will be used.
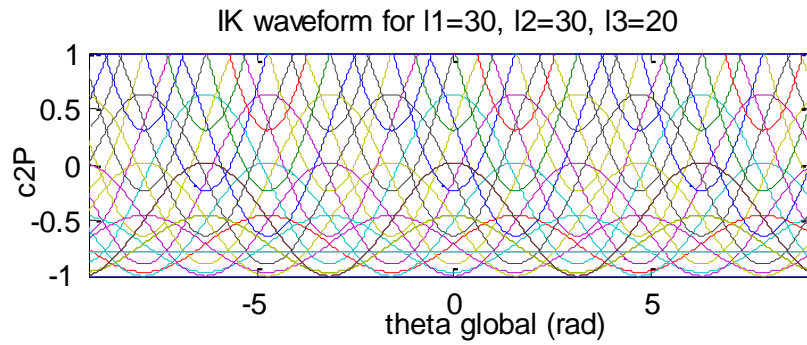

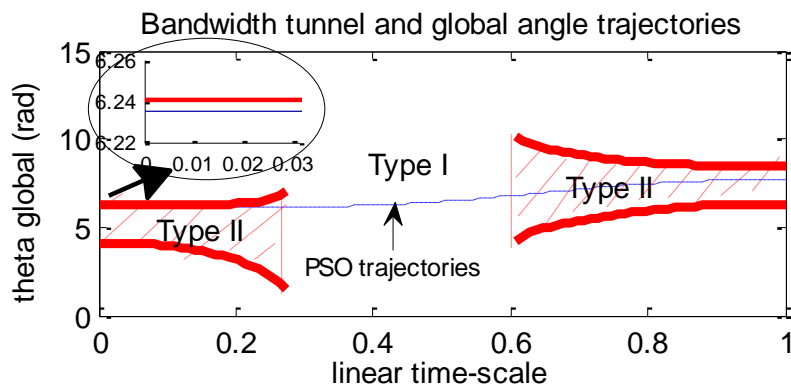Figure 16. Signal generated for l1=30, l2= 30 and l3=20.

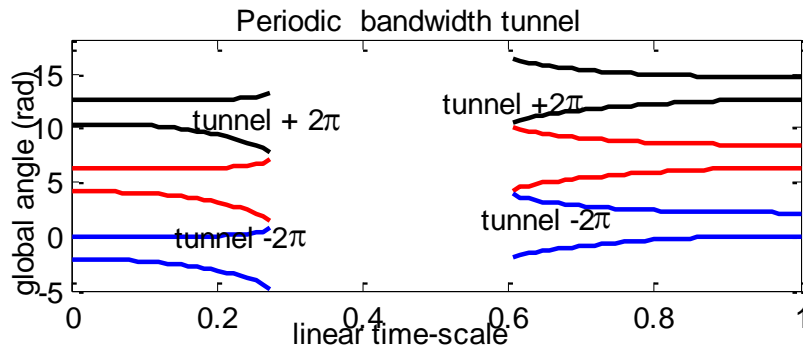Figure 17. Bandwidth tunnel and global angle trajectories.

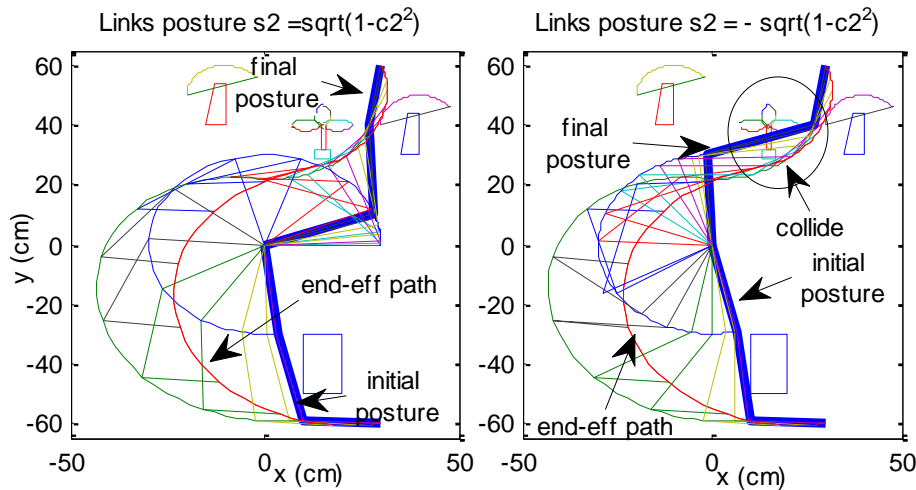Figure 18. Periodic bandwidth tunnel.

Figure 19. Posture change: (a) $s_{2P} = \sqrt{1 - c_{2P}^2}$, (b) $s_{2P} = -\sqrt{1 - c_{2P}^2}$.

To investigate the significant effect of +/- sign of the initial and final global angles, this paper will investigate the IK waveform when the initial or final global angle changes to different +/- sign. Firstly, the final global angle will be changed to θ_{gf}-2π and same a_{6g} will be used. Figure 20 shows global angle trajectories of this change. The trajectories are different from the original one. Consequently, although they give the same end-effector trajectories; however, the motion envelope is different. The motion envelope is the total motion cover by links during tracking the path. These new configurations, as shown in Figure 20, collide with the obstacle. The final and initial configurations are same but the motion envelope is different although it uses same a_{6g} value.
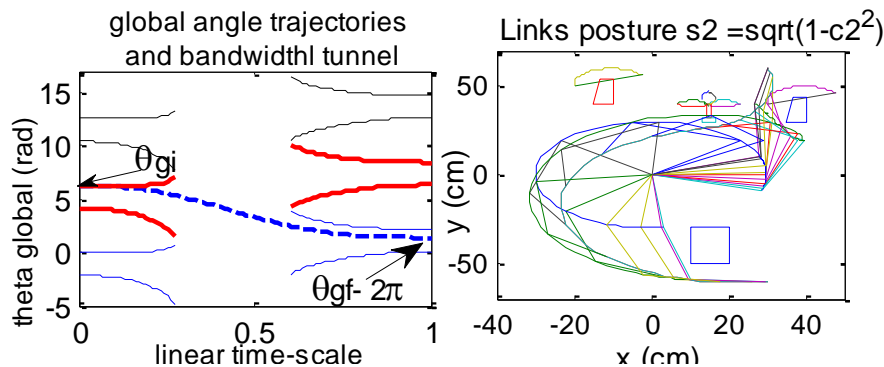

Figure 20. θ_{gf} change to θ_{gf}-2π at similar a_{6g}: (a) tunnel of global angle, (b) postures.

Secondly, this paper will investigate when the initial global angle is changed to $\theta_{gi} - 2\pi$ and the final global angle is same. Using same a_{6g} value, Figure 21 illustrates the global angle trajectories of these initial and final configurations. It shows that beside it collides with the obstacles there is also the trajectories part outside the tunnel. At this part, there will be the tracking error. Generally speaking, different sign of the global angle chosen inside the tunnel, will give different trajectories. Thus, the motion cover by arm robot will also be different, although the end-effector path is same. For avoiding collision, different motion envelope will take significant effect since to avoid collision the motion envelope should be outside the obstacles. The issue is not only end-effector motion but it also considers the motion envelope as the total motion of the arm robot.
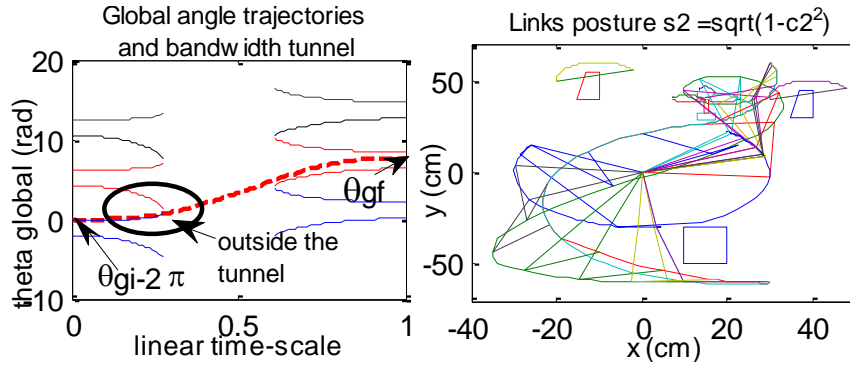
Figure 21. θ_{gi} change to θ_{gi} -2π at similar a_{6g}: (a) tunnel of global angle, (b) postures.

6.2 Tracking Complex Curve , $l_1 = 30$ cm, $l_2 = 30$ cm, $l_3 = 20$ cm

This section will use complex curves to be traced by arm robot using the IK waveform model. The manipulator used is 3-DOF planar series robot and the link lengths are 30 cm, 30 cm and 20 cm for the first, second and third links, respectively. The first complex curve is clothoid [22] which can be expressed in the following

$$x = x_c + \int_0^t k \cos(\tfrac{\pi}{2} t^2) dt$$

$$y = y_c + \int_0^t k \sin(\tfrac{\pi}{2} t^2) dt$$

(27)

where center curve $(x_c, y_c) = (30, 30)$, $k=30$, and t in [0, 3], respectively.

For tracking the clothoid path, the complex waveform will be generated according to Eqs. (11) and (12). The path is divided into 20 parts from the starting point to the final point; the IK waveform for these 20 parts is shown in Figure 22. Because it is periodic, the IK waveform will also be periodic. Interval-limited is chosen as interval of interest. It needs to avoid the ambiguity in choosing the value of θ_g trajectory.
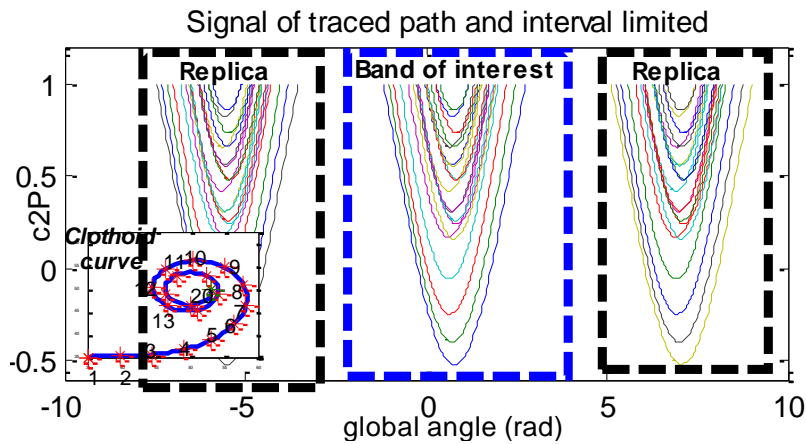

Figure 22. IK waveform of clothoid path.

Figure 23 shows the bandwidth tunnel of this clothoid curve. The polynomial degree sixths for various a_{6g} values are then mapped into the bandwidth tunnel at the initial angle and final angle equal to 1 rad. All a_{6g} values that are inside the tunnel are feasible to be chosen. For example, $a_{6g} = 30$ can be used as trajectories. The posture changes are shown in Figure 24.
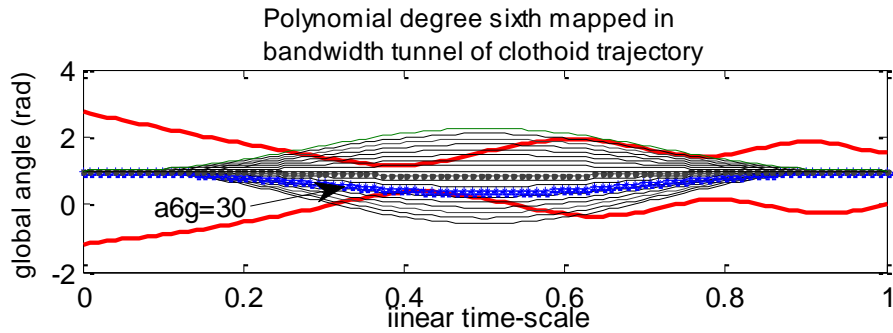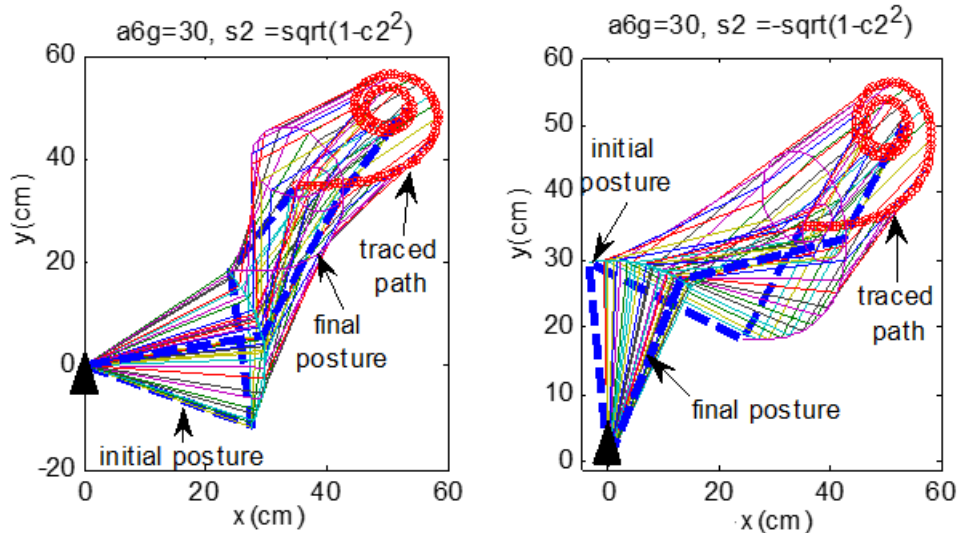
Figure 23. Bandwidth tunnel of clothoid path.

Figure 24. Posture change: (a) $s_{2P} = \sqrt{1 - c_{2P}^2}$, (b) $s_{2P} = -\sqrt{1 - c_{2P}^2}$.

The waveform of tracking this curve is shown in Figure 25. Generally, the signal trajectories should be chosen so that they are connected from the starting point to the final point. Detail of first, second, and third joint angle trajectories is shown in Figure 26.
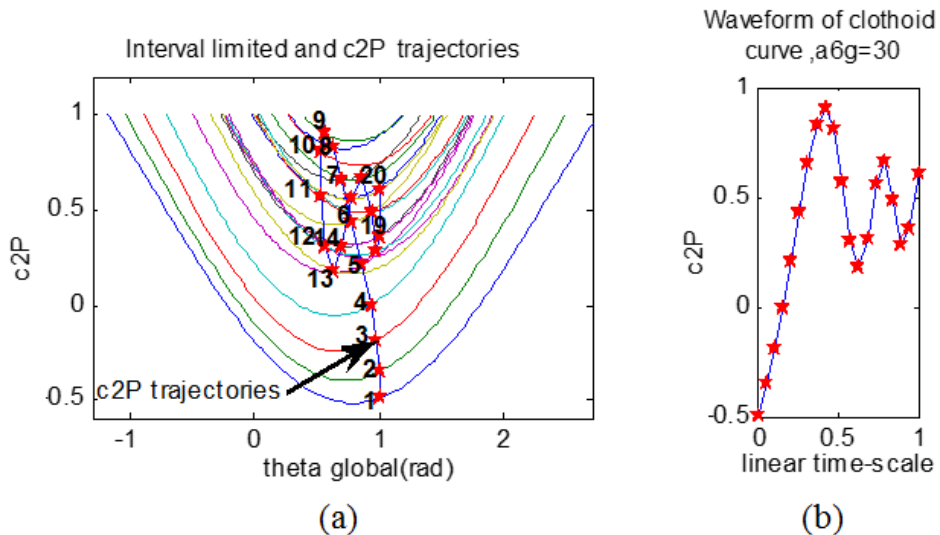

(a)

(b)

Figure 25. Trajectories and waveform of clothoid path for $a_{6g}=30$: (a) IK waveform trajectories, (b) complex waveform generated.
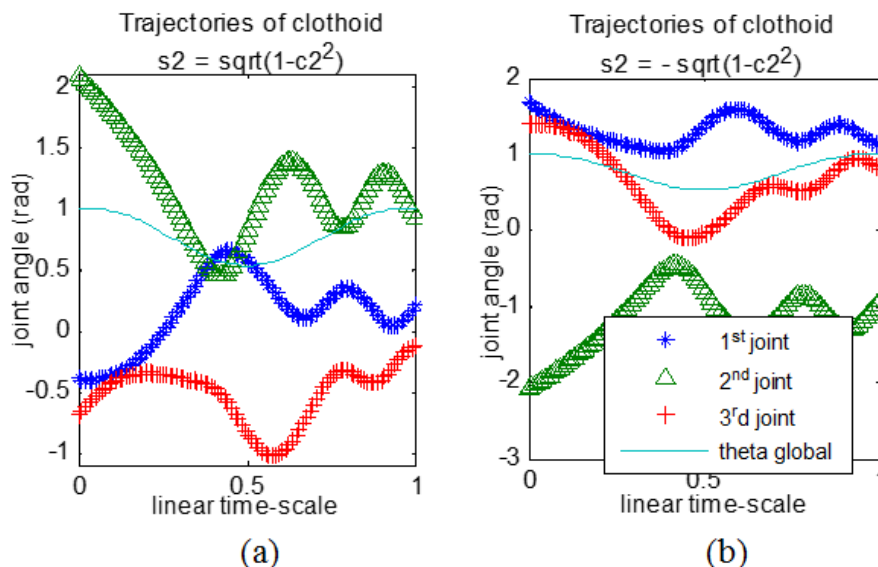
Figure 26. Joint angle trajectories for tracking clothoid path.

Next traced curve is Bezier curve degree fifth with detail of control points are presented in Table 3. This traced path has α-like geometry.

Table 3. Bezier curve tracked path control points of α-like geometry.

B_0	B_1	B_2	B_3	B_4	B_5
(70, 35)	(65, -163)	(45, 0)	(60 , 110)	(65,75)	(70, -35)

Figure 27 shows the bandwidth tunnel of this curve. It shows that the tunnel has complex geometries since there are two throats appear. If the trajectories generation is done directly in one time, there will be no intersection of polynomial degree sixth with the bandwidth tunnel. All trajectories will have parts outside the tunnel
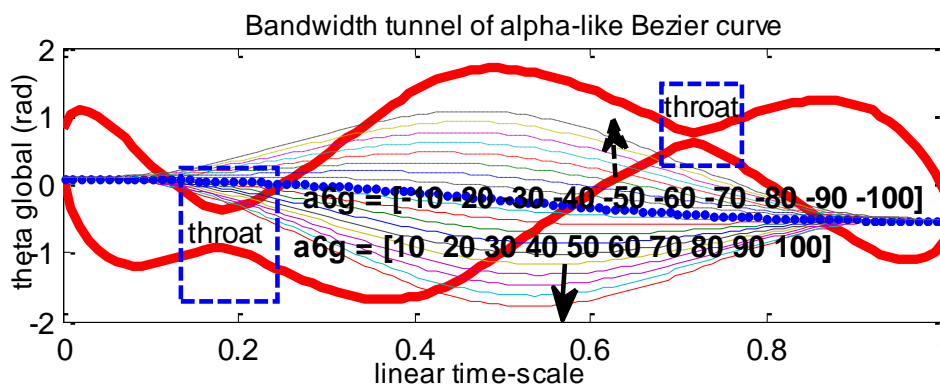

Figure 27. Bandwidth tunnel of α–like curve.

The problem becomes how to keep the trajectories inside the tunnel. At $r = 0.72$, the throat is very small so that the difficulty potentially comes from this point. At this point, the mapping of polynomial degree sixth can be separated. By this scenario, the motion will start at initial point, $r = 0$, and at $r = 0.72$, it will stop for a moment. Then, the second step of motion can be done, from $r = 0.72$ to final point, $r = 1$.

Figure 28 illustrates this scenario. From the initial global angle, which is chosen at $\theta_{gi} = 1.3$ rad and at r=0.72 where the global angle is chosen $\theta_g = 0.7$, $a_{6g} = 110$ or $a_{6g} =$

120 can be used. Figure 29 shows the link postures for the first step with a_{6g}=120. For second step, using $a_{6g} = 30$, the postures are illustrated in Figure 30.
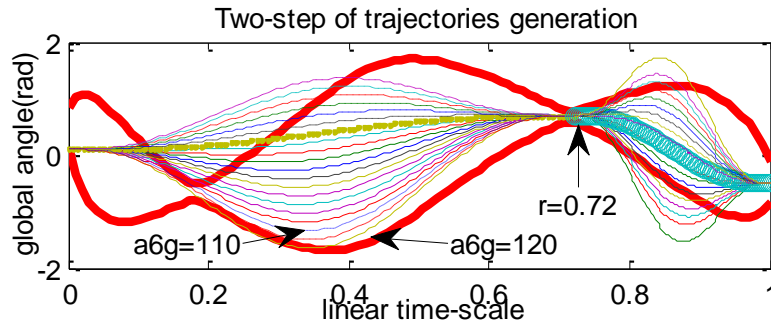
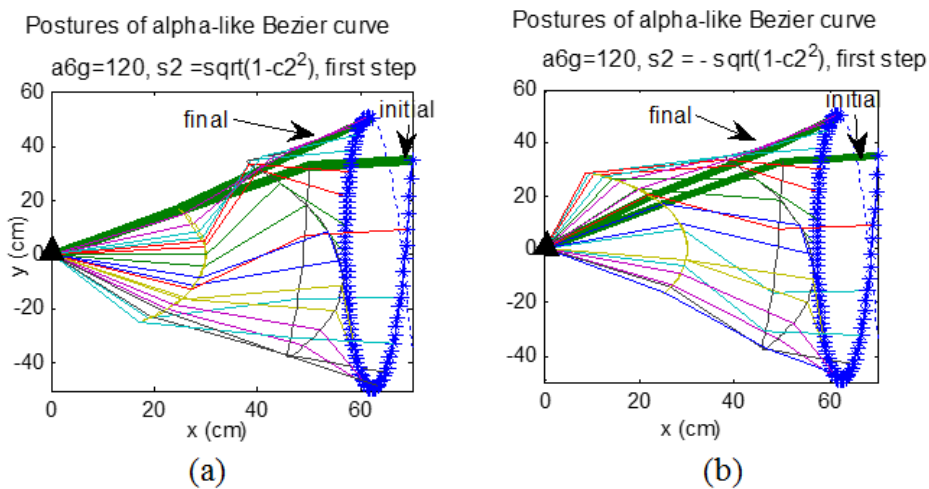

Figure 28. Two steps of trajectories generation.

(a)

(b)

Figure 29. Posture change, first step: (a) $s_{2P} = \sqrt{1 - c_{2P}^2}$, (b) $s_{2P} = -\sqrt{1 - c_{2P}^2}$.
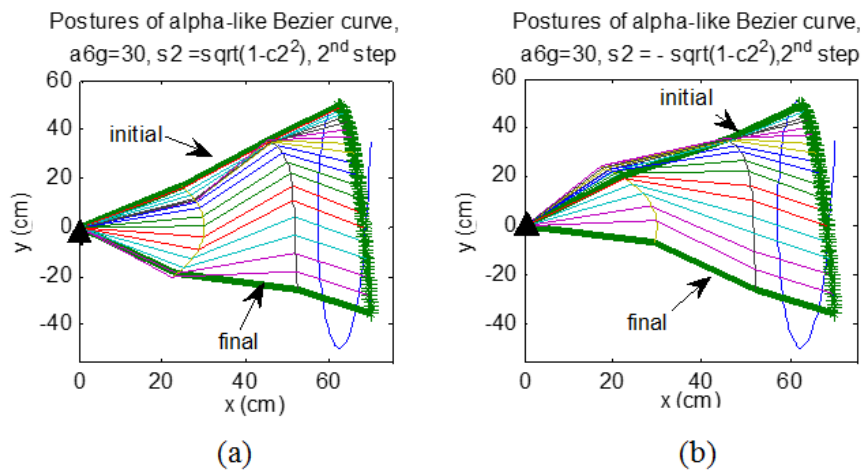

(a)

(b)

Figure 30. Posture change, second step: (a) $s_{2P} = \sqrt{1 - c_{2P}^2}$, (b) $s_{2P} = -\sqrt{1 - c_{2P}^2}$.

6.3 Tracking Complex Curve , $l_1 = 50$ cm, $l_2 = 30$ cm, $l_3 = 40$ cm

The signal generated by the arm robot depends on the arm robot characteristics, which are the link lengths for planar series robot, and the position of point $P(x_P, y_P)$ in the workspace. This section will use different link lengths from previous simulation cases. The first, second, and third lengths used are 50 cm, 30 cm, and 40 cm, respectively. The signals generated in the workspace of the robot are illustrated in Figure 31. Different from the previous link robot, the generated signals consist of all four types of IK waveform.
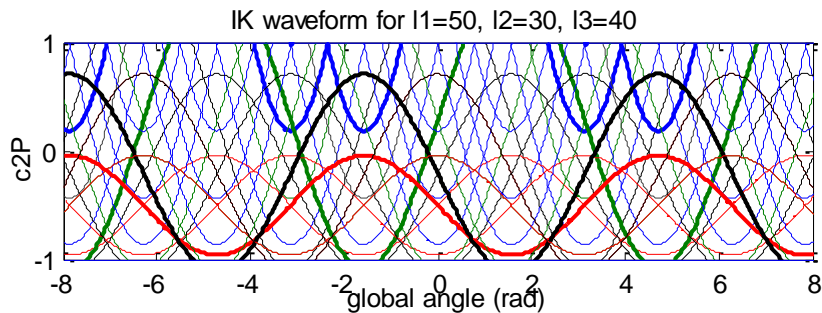

Figure 31. Generated signal for arm robot with $l_1 = 50$ cm, $l_2 = 30$ cm, $l_3 = 40$ cm.

First curve which will be tracked by this robot is the clothoid, with characteristic same with the previous simulation. Although the Cartesian trajectories are same, however, since the link lengths are different, the IK waveform will be different. To track this clothoid, there are two types of the signal generated, i.e. type III and type IV, which construct the bandwidth tunnel as illustrated in Figure 32(b).

Type III has two branches of tunnel which will be separated by a forbidden area. This is due to for type III, there are two bandwidths in single IK waveform. $\theta_{gi} = 1$ cannot be used anymore since it lays in the forbidden area. $\theta_{gi} = 2$ rad and $\theta_{gi} = 0$ rad can be used. With choosing $\theta_{gf} = 1$ rad, these different θ_{gi} values will contribute in different motion envelope, although the end-effector trajectories are same as shown in Figures 32(a) and 32(c). The waveform results using both θ_{gi} values are shown in Figure 33.
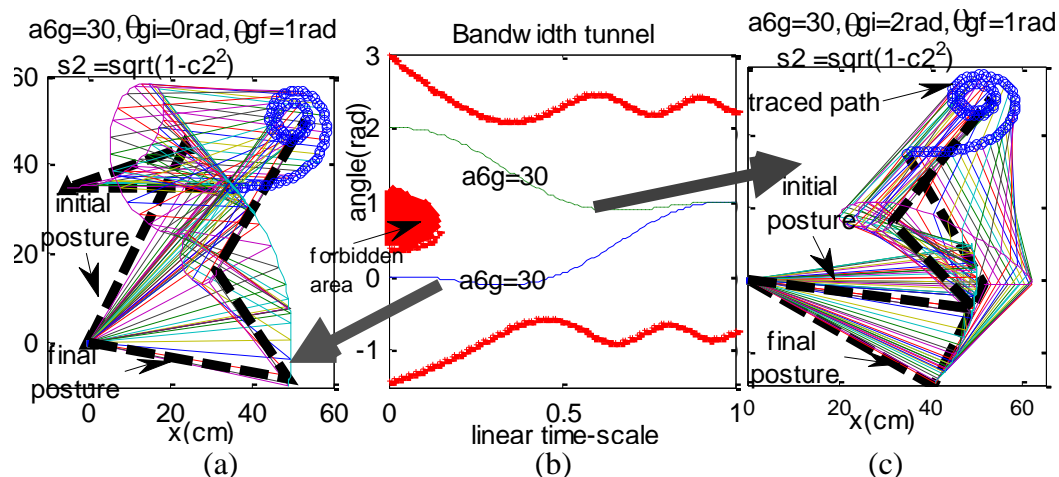

Figure 32. (a) Posture changes for $\theta_{gi} = 0$, (b) bandwidth tunnel, and (c) posture changes for $\theta_{gi} = 1$ rad.
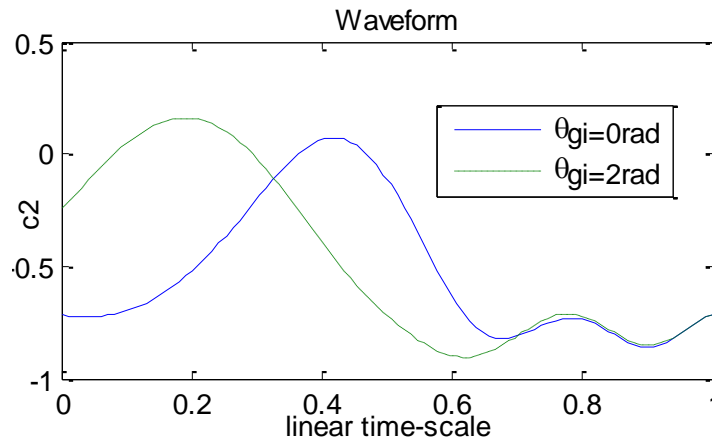
Figure 33. Complex waveform for different value of initial angles.

Next traced path is gear trajectory which has the following equation [21]

$$\begin{cases} x = x_c + k\left(3 + 0.5\sin\left(40\pi t\right)\right)\sin\left(2\pi t\right), \\ y = y_c + k\left(3 + 0.5\sin\left(40\pi t\right)\right)\cos\left(2\pi t\right), \\ \qquad 0 \le t \le 1 \end{cases} \tag{28}$$

where (x_c, y_c) and k are the center of the curve and the scale factor, respectively.

The curve center and k used in this paper are (60, 0) and 5.5, respectively. Figure 34 shows the bandwidth tunnel of this traced curve. The tunnel is very complex consisting of all types of IK waveform. If changing IK waveform type from type III to type IV appears, the tunnel construction should be done carefully. The tunnel should represent the intersection of neighborhood signal so that the feasible region has connectivity as shown in Figure 34.
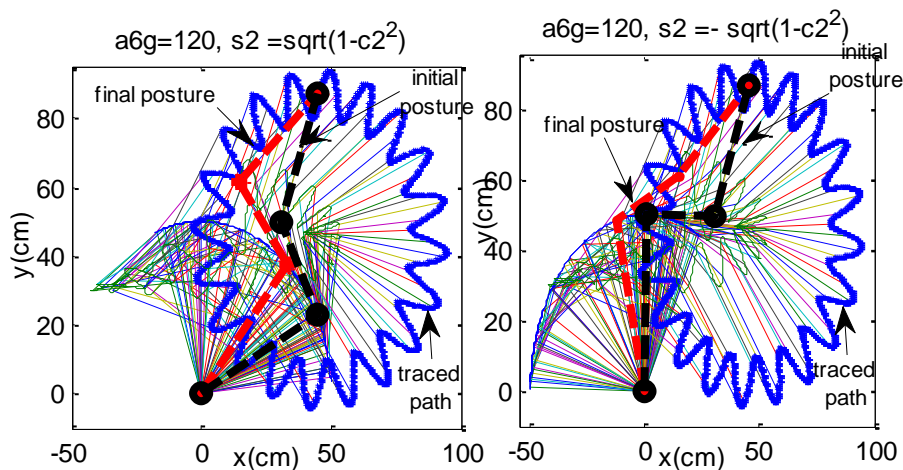

Figure 34. Bandwidth tunnel of gear trajectories.

Type IV will consist of two limited bandwidth of the angle domain. At the tunnel area where this changing type appears, the tunnel is separated into two branches by a forbidden area. The generated trajectories then are possible to be done via upper tunnel or lower tunnel. It is shown that $a_{6g}=120$ lays down inside the bandwidth tunnel. Figure 35 shows the posture changes if this value is chosen to track the gear trajectories.
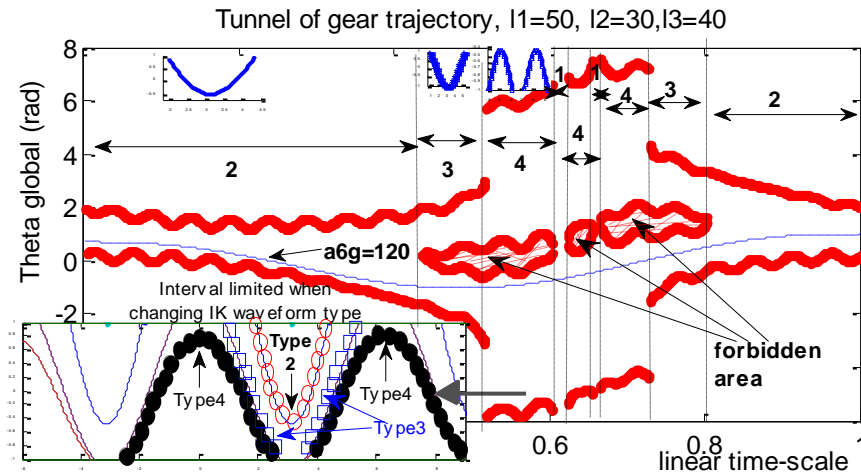
Figure 35. Posture change of gear trajectories: (a) $s_{2P} = \sqrt{1 - c_{2P}^2}$, (b) $s_{2P} = -\sqrt{1 - c_{2P}^2}$.

8. CONCLUSION

Waveform based path tracking of the 3-DOF arm robot manipulator has been presented in this paper. Four types of IK waveform have been described. The specific traced curve will have a unique tunnel of the angle domain which should be computed to visualize the feasible region of path tracking. For tracking the curve, the trajectories should be generated inside the bandwidth tunnel of the angle domain to avoid the position error. In the future works, the path tracking proposed in this paper must be proved to be able to solve trajectories tracking of higher DOF arm robot manipulators.

ACKNOWLEDGEMENT

CONFLICT OF INTERESTS

The authors declare that the there is no conflict of interests regarding the publication of this paper.

REFERENCES

[1] Hormaza LA, Mohammed WM, Ferrer BR, Bejarano R and Lastra JLM. On-line Training and Monitoring of Robot Tasks through Virtual Reality. In: 2019 IEEE 17th International Conference on Industrial Informatics (INDIN), Helsinki, Finland, 22-25 July 2019.

[2] Ovchinnikov I, Kovalenko P. Predictive Model to Simulate Humanoid Gait. In: International Journal of Innovative Technology and Interdisciplinary Sciences, 2018, Vol 1(1), pp. 9-17.

[3] Pac MR, Popa DO. Interval analysis of kinematic error in serial manipulator using product of exponential formula. In: IEEE Trans. Autom. Sci. Eng., 2013, Vol. 10, pp. 525-535.

[4] Almarkhi AA, Maciejewski AA. Singularity Analysis for Redundant Manipulators of Arbitrary Kinematic Structure. In: Proceedings of the 16th International Conference

on Informatics in Control, Automation and Robotics (ICINCO 2019) - Volume 2, pages 42-49.

[5] Wampler CW. Inverse kinematic function for redundant manipulators. In: Proceedings IEEE Conf. Robotics and Automat*.,* 1987, pp. 610–617.

[6] Baillieul J. Kinematic programming alternatives for redundant manipulators. In: Proceedings IEEE Conf. Robotics and automation, 1985. pp. 722–8.

[7] Baker DR, Wampler CW. On the inverse kinematics of redundant robot manipulators. In: Int. J. Robot. Res., 1988, vol 7, pp. 3-21.

[8] Burdick JW. On the inverse kinematics of redundant manipulators: characterization of the self-motion manifolds. In: Proc. IEEE Conf. Robotics and Automat. Scottsdale, Arizona, 1989, pp. 264-270.

[9] Ahuactzin JM, Gupta K. A motion planning based approach for inverse kinematics of redundant robots: the kinematic roadmap. In: Int. J. Robot. Res., 1998, vol 14, pp. 159-167.

[10] Nerchou AC. Solving the inverse kinematics problem of redundant robots operating in complex environments via modified genetic algorithm. In: Mech. Mach. Theory, 1998, vol 33, pp. 273-292.

[11] Marcos MG, Machado JAT, Azavedo-Perdicoulis TP. Trajectory planning of redundant manipulators using genetic algorithms. In: Commun. Nonlinear Sciences, 2009, vol 14, pp. 2858-2869.

[12] Rao RS, Asaithambi A, Agraval SK. Inverse kinematic solution of robot manipulators using interval analysis. In: J. Mech. Des., 1998, vol 120, pp. 147-150.

[13] Pac MR, Popa DO. Interval analysis of kinematic error in serial manipulator using product of exponential formula. In: IEEE Trans. Autom. Sci. Eng., 2013, Vol. 10, pp. 525-535.

[14] Wei Y, Jian S, He S, Wang Z. General approach for inverse kinematics of nR robots. In: Mech. Mach. Theory, 2014, vol 75, pp. 97-106.

[15] Rudny T. Solving inverse kinematics by fully automated planar curves intersecting. In: Mech. Mach. Theory, 2014, vol 74, pp. 310-318.

[16] Toz M. Chaos-based Vortex Search algorithm for solving inverse kinematics problem of serial robot manipulators with offset wrist. In: Applied Soft Computing Volume 89, April 2020, 106074.

[17] Erleben K, Andrews S. Solving inverse kinematics using exact Hessian matrices. In: Computers & Graphics, 2019, Volume 78, pp. 1-11.

[18] Dereli S, Köker R. A meta-heuristic proposal for inverse kinematics solution of 7-DOF serial robotic manipulator: quantum behaved particle swarm algorithm. In: Artificial Intelligence Review, 2020, volume 53, pages949–964.

[19] Pan X, Polden J, Larkin N, Duin SV, and Norrish J. Recent progress on programming methods for industrial robots. In: Robot. Comput.-Integr. Manuf, 2012, vol. 28, pp. 87-94.

[20] Orfanidis SJ. Introduction to Signal Processing. Pearson Education, Inc. 2010.

[21] Machmudah A, Parman S, Zainuddin A, Chacko S. Polynomial joint angle arm robot motion planning in complex geometrical obstacles. In: Applied Soft Computing, 2013, vol 13, pp. 1099-1109.

[22] Merlet JP. A generic trajectory verifier for the motion planning of parallel robot. In: Journal of Mechanical Design, 2001, vol. 123, pp. 510-515.

Appendix A

Obstacle coordinates from [7] to be used in this paper.